coatings

MDPI

Article

Influence of Niobium Substitution on the Properties of $Pb_2Fe_2O_5$ Thin Films Synthesized via Reactive Magnetron Sputtering

Benas Beklešovas, Vytautas Stankus * and Aleksandras Iljinas

Department of Physics, Kaunas University of Technology, Studentu Str. 50, LT-51368 Kaunas, Lithuania; beklesovas@gmail.com (B.B.); aleksandras.iljinas@ktu.lt (A.I.)
* Correspondence: vytautas.stankus@ktu.lt

Abstract

Lead ferrite ($Pb_2Fe_2O_5$) is a promising multiferroic material that exhibits both ferroelectric and magnetic properties at room temperature. This study investigates how substituting niobium and adjusting the synthesis temperature affect the structural, morphological, and ferroelectric properties of lead ferrite thin films deposited via reactive magnetron sputtering. Niobium-substituted PFO films ($Pb_2Fe_{2(1-x)}Nb_{2x}O_5$), where x corresponds to Nb_2O_5 contents of 3 wt.%, 5 wt.% and 10 wt.%, were prepared for this study, and denoted as PFONb3, PFONb5 and PFONb10, respectively. X-ray diffraction analysis confirmed the formation of Nb-substituted PFO phases, while polarization–electric field measurements demonstrated an increase in remnant polarization (P_r), with higher Nb content reaching a maximum P_r of 65 $\mu C/cm^2$ at 10 wt.% Nb and a substrate temperature of 500 °C. Scanning electron microscopy and energy-dispersive spectroscopy revealed a uniform distribution of elements and a well-defined surface structure. These results highlight the need to fine tune synthesis parameters, such as temperature and substitution concentrations, to achieve optimal ferroelectric characteristics.

Keywords: ferroelectrics; $Pb_2Fe_2O_5$; multiferroic; niobium-substituted; reactive magnetron sputtering

Academic Editor: Andrey V. Osipov

Received: 18 April 2025
Revised: 7 July 2025
Accepted: 19 July 2025
Published: 23 July 2025

Citation: Beklešovas, B.; Stankus, V.; Iljinas, A. Influence of Niobium Substitution on the Properties of $Pb_2Fe_2O_5$ Thin Films Synthesized via Reactive Magnetron Sputtering. *Coatings* **2025**, *15*, 863. https://doi.org/10.3390/coatings15080863

1. Introduction

Materials in which electric and magnetic interactions occur simultaneously, related to the crystal structure of the material, are called multiferroics [1–4]. These materials ($BiFeO_3$ (BFO) [5], $CoFe_2O_4$ [6], $BiMnO_3$ [7], $YMnO_3$ [8,9]) have aroused great interest and optimism in considering the possibilities of elucidating the mechanism of these interactions, thereby facilitating fundamental discoveries. The properties manifested in these materials have given rise to countless ideas on how to use them in next-generation electronics (spintronics), sensors, and solar cell applications [10–12]. Among them, a new generation of memory devices that can be electrically written and magnetically read [13–15], due to their high-speed operation and low energy consumption, could change the memory market drastically. However, these hopes face challenges because in most multiferroics characterized by acceptable polarization values, the magnetoelectric coupling is very weak, or strong coupling appears in materials with a weak dielectric polarization. Even the most widely studied bismuth ferrite has not yet met all the expectations placed on it due to the overlap interactions of nearby memory cells and excessive leakage currents [5]. Therefore, materials with strong magnetoelectric coupling and that are acceptable for practical application of their electrical and magnetic properties at room temperature are one of the

main tasks of materials science [16]. One such material as a potential candidate could be ($Pb_2Fe_2O_5$) thin films substituted by various rare or transitional elements. In our previous work, we demonstrated the successful substitution of Fe^{3+} ions with Cr [17], Co [18] and Ni [19] ions and the enhancement of multiferroic properties in PFO thin films. Crystal structure, morphology, and thickness, which influence electrical and magnetic properties of thin films, depend greatly on the method and parameters of phase growth, such as reactive plasma conditions, deposition temperature, sputtering rate, ratio of deposited flows of atoms coming from sputtered targets, etc. [17–19].

This work's aim is to synthesize niobium-substituted lead ferrite thin films and examine how the deposition temperature and concentration of niobium affect the thin films' ferroelectric characteristics, crystal structure, and surface morphology. Niobium-substituted lead ferrite ($Pb_2Fe_2O_5$) thin films are presented in this work as a unique method to improve the ferroelectric characteristics of multiferroics at room temperature. The results give fresh information about substitution techniques that can greatly enhance the ferroelectric characteristics, which are essential for real-world uses.

2. Materials and Methods

Niobium-substituted $Pb_2Fe_2O_5$ (PFO) thin films were synthesized by the reactive magnetron sputtering deposition using layer-by-layer method. The films were deposited on a platinized silicon substrate, consisting of a multilayer system of $Pt/Ti/SiO_2/Si$ with respective thicknesses of 200 nm, 20 nm, 1 μm, and 380 μm (Nanoshel Company, Cheshire, UK). Platinized silicon was chosen for its excellent properties, including platinum's chemical inertness, thermal expansion compatibility with ferroelectric films, and suitable crystal lattice [20–22]. Each element—lead (Pb), iron (Fe), and niobium (Nb)—was deposited using a dedicated magnetron equipped with high-purity targets (99.9%, 3-inch disc-shaped; Kurt J. Lesker Company, Dresden, Germany). A 60 mm distance between the target and substrate was set. A semi-circular moving path of the substrate above the three separate targets was maintained throughout the synthesis process with a period of 2 s. To enhance the adhesion of the PFO thin films to the substrate, a 5 nm titanium seeding layer was deposited at 750 °C in an argon atmosphere with a pressure of 1.3 Pa [23]. After the seeding layer was formed, the substrate temperature was reduced to one of three deposition temperatures: 500 °C, 550 °C, or 600 °C. The process gas was switched to oxygen. The niobium concentration in the PFO thin films was precisely controlled using an adjustable aperture, placed over niobium target. The thin films deposition time was 60 min. Once the process was complete, planar capacitors were formed with platinum as the bottom electrode and a top Al electrode, which were deposited through via the thermal evaporation method on the PFO film through a mask with 1.5 mm circular holes.

To control Nb concentration, the deposition rate of Nb oxide (Nb_2O_5) was determined by measuring the thickness of the films and calculating using volume, density and mass. The following chemical Equation (1) was used to determine the Nb concentration (wt.%) in films:

$$2PbO + (1-x)Fe_2O_3 + xNb_2O_5 \overset{t=500\ ^\circ C-600\ ^\circ C}{\rightarrow} Pb_2Fe_{2(1-x)}Nb_{2x}O_5 \quad (1)$$

Niobium substituted PFO films ($Pb_2Fe_{2(1-x)}Nb_{2x}O_5$), where x corresponds to Nb_2O_5 contents of 3 wt.%, 5 wt.% and 10 wt.%, were prepared for this study, and denoted as PFONb3, PFONb5 and PFONb10, respectively.

To analyze the structural properties of the PFO films, X-ray diffraction (XRD) measurements was performed using a Bruker D8 diffractometer (Bruker, Billerica, MA, USA) with monochromatic CuKα radiation in Bragg–Brentano geometry. The Sawyer–Tower method, using a circuit with a 1 kΩ resistor and a 150 nF reference capacitor at 50 Hz, under

ambient conditions (20 °C), was utilized for ferroelectric hysteresis loop measurements. For surface morphology analysis, the scanning electron microscope (S-3400N, Hitachi, Tokyo, Japan) operated at 10 kV was used. The elemental distribution of Fe, Pb, Nb, and O within the films was determined by energy-dispersive spectroscopy (EDS) using a Bruker Quad 5040 spectrometer (AXS Microanalysis GmbH, Hamburg, Germany).

3. Results and Discussion

3.1. XRD Analysis

The comparison of XRD spectra of PFO substituted with different niobium concentrations, synthesized at the same temperature of 500 °C, is presented in Figure 1. These samples were selected for the XRD analysis because, as will be demonstrated later in this paper, the best ferroelectric parameters were recorded at this synthesis temperature. The peaks of the following PFO phases (220), (312), (400), and (424) are detected at 2θ angles of approximately 32°, 38°, 46°, and 56°, respectively [24]. It is noted that the PFO peaks are slightly shifted to higher 2θ angles in all Nb-doped samples compared to the undoped PFO. This consistent shift may indicate a minor lattice contraction or strain introduced by the initial incorporation of Nb into the PFO lattice. Due to the small difference in ionic radii between Fe^{3+} and Nb^{5+}, the effect appears subtle and likely localized, rather than reflecting a uniform change in lattice parameters across compositions [25,26].

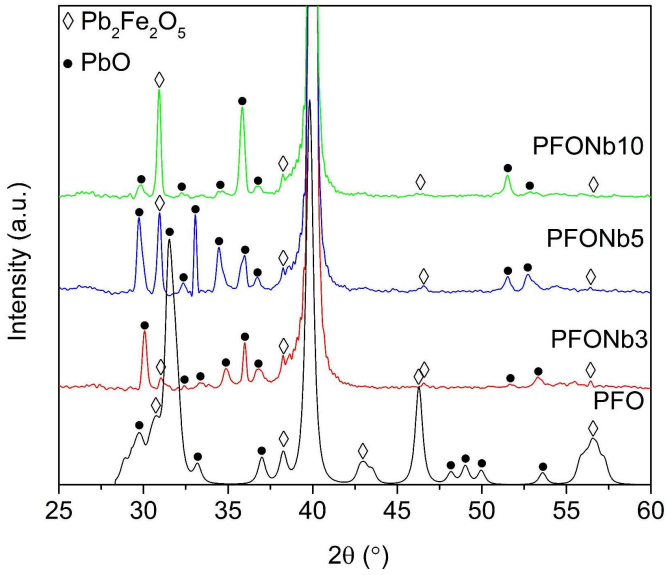

Figure 1. Comparison of XRD spectra of Nb-substituted PFO thin films with varying Nb concentrations synthesized at 500 °C.

As with other samples, several peaks of PbO phases are detected at 2θ angles of approximately 30°, 33°, 34°, 35°, 36°, 52°, and 53°. The intensities of the PbO peaks also vary with changes in niobium concentration, but no linear relationship with the concentration is observed. A.M. Abakumov [27] and M. Wang [28] have shown that the synthesis process leads to the formation of crystallographic planes, which results in variations in the chemical formula of lead ferrite, represented as $Pb_{0.9375}FeO_{2.4375}$, $Pb_{0.9}FeO_{2.4}$, and $Pb_{0.875}FeO_{2.375}$. These variations are generalized by the formula $PbFeO_{2.5-x}PbO$, where x equals 0.0625, 0.1, and 0.125. This supports the view that secondary PbO phases are nearly unavoidable during synthesis, as reflected in the XRD spectrum in Figure 1. While PbO peaks are present, the simultaneous detection of characteristic PFO reflections (such as the (220), (312), (400) and (424) peaks) confirms the formation of the desired phase. In complex oxide thin films, secondary PbO phases can form due to local stoichiometric imbalance, promoting

lead enrichment or PbO segregation. The synthesis temperature of 500 °C may contribute to partial lead volatilization, further affecting the PbO phase behavior. The increase in remnant polarization with Nb concentration further supports that the PFO phase remains the primary contributor to the observed ferroelectric properties.

A comparison of the XRD spectra for PFONb10, coatings synthesized at temperatures ranging from 500 to 600 °C is presented in Figure 2. The PFONb10 was selected for this analysis because it represents the highest Nb concentration used for substitution in PFO films, which increases the likelihood of observing structural changes in the material. The lead ferrite phase peaks (220), (312), and (424) are detected at 2θ angles of approximately 32°, 38°, and 56°, respectively [24]. With increasing synthesis temperature, the observed decrease in the intensity of the PFO (220) peak suggests microstructural modifications, likely influenced by lead volatilization. The selective nature of this intensity change likely reflects anisotropic crystal growth behavior, where certain crystallographic planes become more or less dominant depending on the synthesis conditions. Peaks consistent with Nb_2O_5 are observed at $2\theta \approx 33.5°$ in the XRD patterns of all samples, regardless of synthesis temperature.

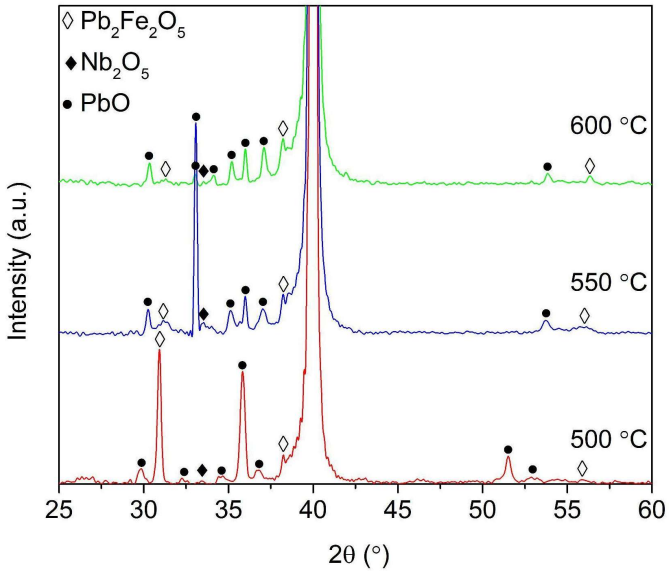

Figure 2. Comparison of XRD spectra of PFONb10 thin films synthesized at different temperatures.

Alongside the PFO and niobium oxide phases, PbO phase peaks were also identified, located at 2θ angles of approximately 30°, 33°, 34°, 35°, 36°, 37°, 51.5°, and 53°. The intensity of these peaks varies only slightly with changes in synthesis temperature, except for the peaks at 33°, 36° and 52° 2θ, which decrease as the temperature increases. This selective reduction in intensity may not indicate the complete removal of the PbO phase, but rather a redistribution or partial decomposition of Pb-containing phases due to temperature-driven lead volatilization. Such localized changes are consistent with observations in lead-based oxide thin films, where minor Pb loss or redistribution can occur without uniformly suppressing all PbO-related reflections [29].

XRD results suggest that Nb is at least partially incorporated into the PFO lattice, likely substituting for Fe^{3+}. However, the appearance of a distinct peak at 33.5°, consistent with Nb_2O_5, particularly in the PFONb5 sample, indicates that some Nb may also form a separate phase. This suggests that both substitution and secondary phase formation may occur simultaneously, depending on the Nb concentration and synthesis conditions.

3.2. Ferroelectric Properties

Figure 3 presents the comparison of polarization dependency on the electric field (50 Hz) for coatings deposited at different temperatures and niobium concentrations at room temperature. In Figure 3a, the family of hysteresis loops is shown for PFO coatings formed at the same synthesis temperature of 500 °C with varying niobium concentrations. It should be noted that below a 500 °C deposition temperature, no ferroelectric phase was observed. None of the hysteresis loops reached polarization saturation or exhibited an oval-shaped dependency. This may be attributed to leakage currents caused by oxygen vacancies and other defects in the samples. Despite the presence of leakage currents in the coatings, a noticeable increase in remnant polarization and coercive field values with Nb concentration is observed. This effect can be attributed to Nb^{5+} substitution for Fe^{3+}, introducing a charge imbalance that alters the defect chemistry of the material. Nb doping is known to suppress the formation of oxygen vacancies, which are the source of leakage current and domain wall pinning, by charge compensation mechanisms. As a result, domain switching becomes more stable and ferroelectric performance improves. The introduction of Nb also promotes the formation of A-site (Pb-site) vacancies, which relieve local mechanical stress during polarization reversal and support easier domain wall movement [30]. With a further increase in Nb content (above 10%), the hysteresis displayed unchanged ferroelectric properties.

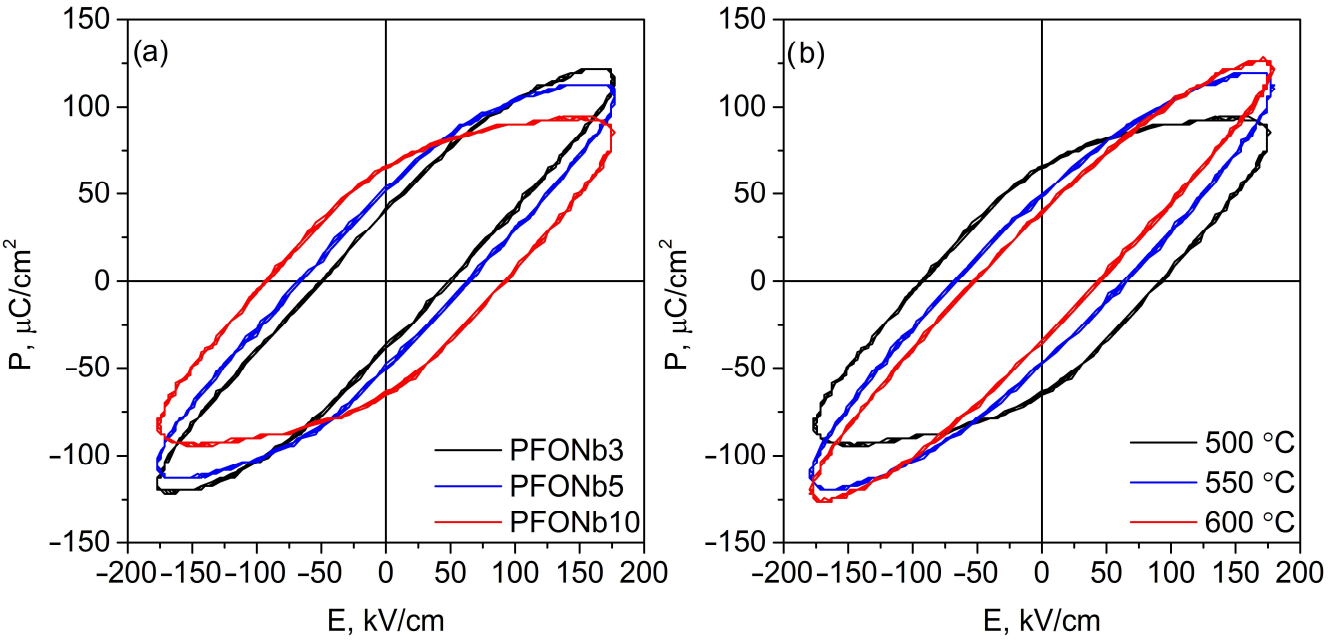

Figure 3. Comparison of P–E curves: effect of niobium concentration on substituted PFO, deposited at 500 °C (**a**), and the synthesis temperature influence on PFONb10 samples (**b**).

In Figure 3b, the comparison of polarization hysteresis loops is presented for PFONb10 coatings synthesized at different temperatures. The hysteresis loops of the coatings maintain an oval shape, like the previous samples, and leakage currents could not be avoided. As the synthesis temperature increases, a decline in ferroelectric parameters is observed, reflected in the elongated and oval shape of the hysteresis loops. Both remnant polarization and coercive field values decrease accordingly: P_r from 65 μC/cm^2 to 40 μC/cm^2, and E_c from 92 kV/cm to 46 kV/cm. Unlike the P_r and E_c values, higher polarization saturation values are recorded at elevated synthesis temperatures (600 °C), reaching approximately 125 kV/cm, compared to 90 kV/cm in the film formed at 500 °C.

Figure 4 presents a comparison of the influence of synthesis temperature and Nb content in the PFO films. In Figure 4a, the comparison of ferroelectric parameters between PFO coatings formed at different temperatures with the same Nb content is shown. As observed in the hysteresis loops, this comparison also reveals a decrease in Pr and Ec values as the synthesis temperature increases. For the PFONb10 coating, Pr decreased from 65 μC/cm^2 to 49 μC/cm^2 and then to 41 μC/cm^2 at 500 °C, 550 °C, and 600 °C, respectively. The Ec value exhibits a similar trend, changing from 92 kV/cm to 63 kV/cm and then to 45 kV/cm at the same respective temperatures. The change in ferroelectric parameters is likely influenced by partial lead volatilization during synthesis at higher temperatures, as commonly reported for lead-based perovskites [29]. The lead evaporation may result in an increased concentration of defects, which disrupts the long-range ferroelectric order, affecting film polarization as well.

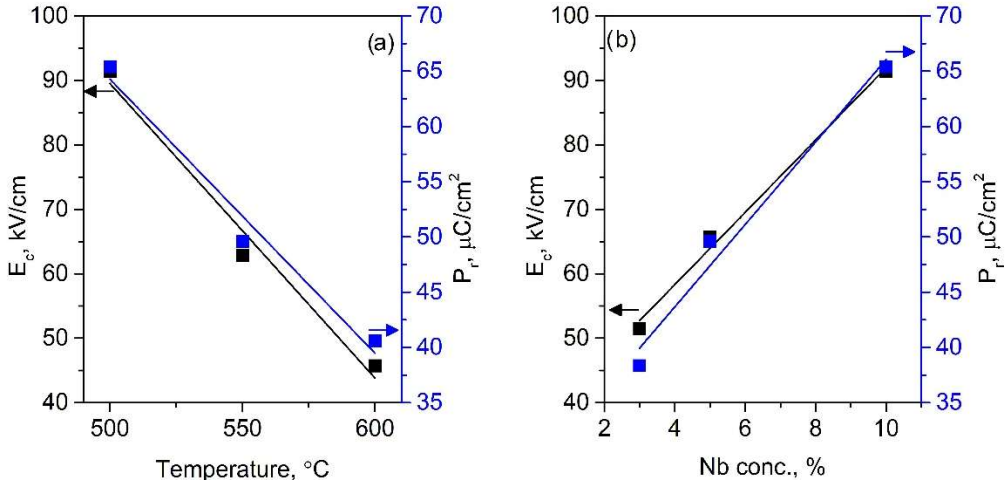

Figure 4. PFONb10 film properties as a function of synthesis temperature (**a**) and effects of niobium concentration on the ferroelectric properties of PFO films synthesized at 500 °C (**b**).

Figure 4b analyzes the influence of niobium content on the ferroelectric properties of PFO thin films. A positive trend is observed as the niobium concentration in the coatings increases. For the PFONb3, PFONb5, and PFONb10 samples, the achieved P_r values were 38 μC/cm^2, 49 μC/cm^2, and 65 μC/cm^2, respectively, while the E_c values changed to 51 kV/cm, 66 kV/cm, and 91 kV/cm. Remnant polarization increased by 75%, which can be attributed to the substitution of smaller Fe^{3+} ions (RFe^{3+} = 0.065 nm) with larger Nb^{5+} ions (RNb^{5+} = 0.072 nm) [25]. Although this difference is small, it can introduce localized lattice distortions that enhance dipole alignment, thereby contributing to improved ferroelectric polarization. The incorporation of Nb^{5+} into iron-based perovskites is reported to influence the valence state of Fe ions and reduce oxygen vacancy concentrations [31,32]. Nb^{5+} substitution can partially reduce Fe^{3+} to Fe^{2+} due to charge compensation mechanisms, with Fe^{2+} having a larger ionic radius, which introduces additional lattice distortion and enhances the dipole moment. This effect, along with suppressed oxygen vacancy formation, contributes to improved ferroelectric ordering and increased remnant polarization [31,32]. Excessive reduction of Fe^{3+} can lead to charge imbalance, potentially introducing localized states that trap carriers and increase leakage currents. For this reason, the optimized Nb substitution for the PFO films is crucial to enhancing ferroelectric performance [31,32].

3.3. Morphology

Figure 5 shows SEM images of PFONb10 coatings deposited at synthesis temperatures ranging from 500 °C to 600 °C. In the sample formed at 500 °C (Figure 5a), closely packed, stacked straw structures with well-defined boundaries are observed. At 550 °C (Figure 5b),

the size and shape of the structures remain consistent, but their arrangement becomes more compact. At 600 °C (Figure 5c), some of these columnar structures retain the morphology seen at 550 °C, while others grow noticeably larger, suggesting increased atomic mobility and coarsening effects at higher temperatures [33,34].

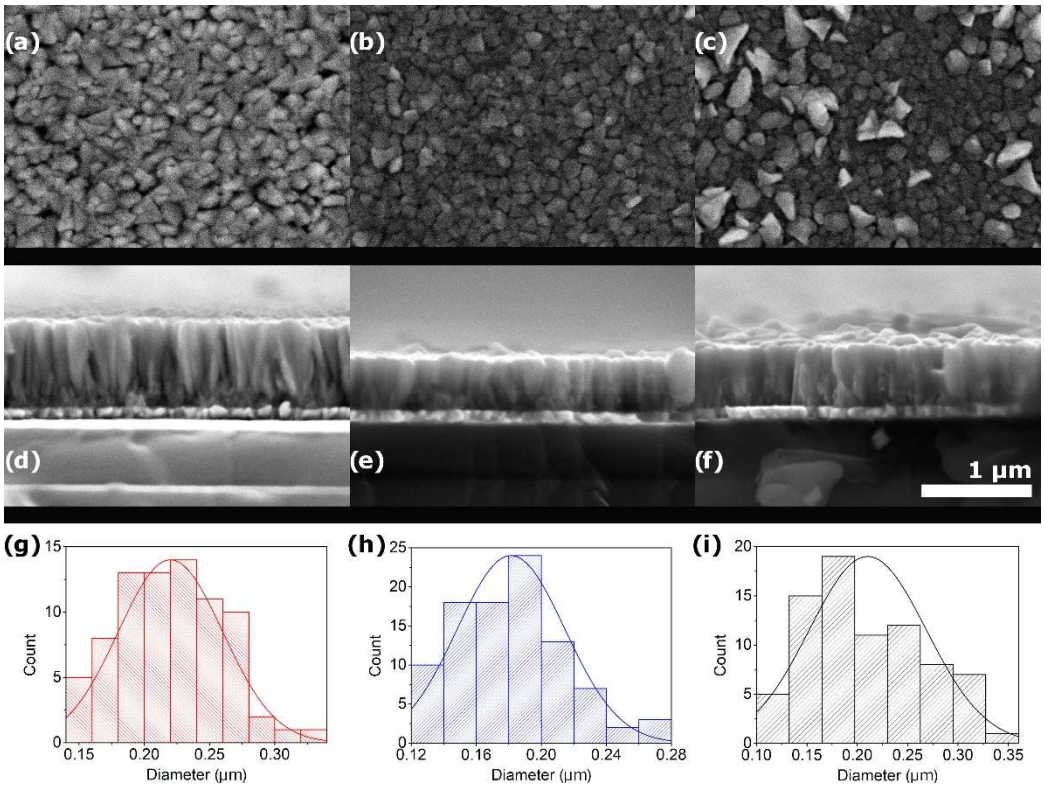

Figure 5. Surface and cross-sectional SEM views of PFONb10 films formed at (**a**,**d**) 500 °C, (**b**,**e**) 550 °C, and (**c**,**f**) 600 °C with column diameter distribution shown in (**g**–**i**).

Figure 5d–f shows a cross-sectional view of the PFONb10 films synthesized at a 500 °C to 600 °C temperature range. Columnar structures that widen in diameter along the growth direction are observed in all samples. The smaller structures are also present between the larger columns in all samples, but are more pronounced in the sample synthesized at 500 °C (Figure 5d), likely due to the lower synthesis temperature. As atoms reach the surface, they tend to attach laterally to the sides of the growing columns. The ion flux may also contribute to such an arrangement. This is attributed to the semicircular path of the substrate over the magnetron, which leads to the deposition of atoms from various directions, resulting in lateral atom localization on the column sides and shadowing adjacent columns [35]. At 550 °C (Figure 5e), the more compact column arrangement is observed. Although the surface structures measured at this temperature are smaller, this could be related to the column formation, where diameters increase along the growth direction. At 600 °C (Figure 5f), the columns display similar characteristics to those at 550 °C, as confirmed by surface images showing partially identical coating structures. However, larger columnar structures are observed at 600 °C. The thicknesses of the films deposited at 500 °C, 550 °C, and 600 °C are 790 nm, 490 nm, and 530 nm, respectively. The slightly increased thickness at 600 °C, compared to the 550 °C sample, may be attributed to continued vertical column growth or increased atomic mobility, which supports the formation of both taller and coarser surface structures [33,35].

In Figure 5g–i, the surface structure size distribution is presented. At synthesis temperatures of 500 °C, 550 °C, and 600 °C, the sizes of the columnar structures are approximately

220 nm, 181 nm, and 210 nm, respectively. Although the column width does not change significantly with increasing temperature, it is observed that surface diffusion facilitates a more compact arrangement of columns.

Figure 6 represents the elemental composition of a PFONb10 film synthesized at 550 °C. The Fe and Pb elements appear uniformly distributed across the sample's surface, with no visible irregularities. A similar distribution is observed for the Nb element, although its occurrence is less frequent. The EDS mapping confirms a consistent dispersion of lead, niobium, and oxygen throughout the film. The niobium content was quantified at 9.9 ± 0.2 wt.%, while oxygen constituted 16.9 ± 0.8 wt.%. Iron and lead were present at 25.5 ± 0.8 wt.% and 47.6 ± 1.2 wt.%, respectively.

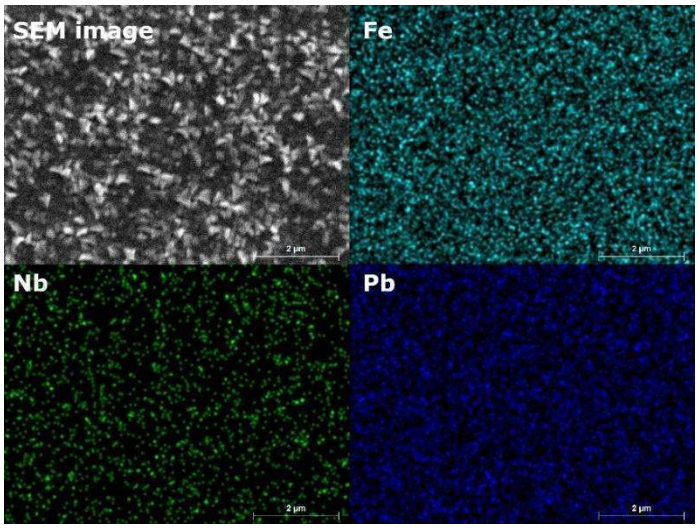

Figure 6. EDX mapping of the PFONb10 film synthesized at 500 °C.

4. Conclusions

The structural, ferroelectric, and morphological properties of niobium-substituted PFO thin films synthesized under varying niobium concentrations and synthesis temperatures were investigated. The results show that niobium incorporation in PFO thin films significantly influences their structural and ferroelectric behavior. According to XRD analysis, niobium substitution affects the intensity of PFO phase peaks, but does not prevent the formation of secondary phases, such as PbO and Nb_2O_5. Ferroelectric measurements displayed a positive correlation between Nb content and remnant polarization, with P_r increasing from 38 $\mu C/cm^2$ (PFONb3) to 65 $\mu C/cm^2$ (PFONb10). In contrast, increasing the synthesis temperature from 500 °C to 600 °C led to a decline in ferroelectric performance, likely due to lead volatilization and temperature-induced structural alterations that disturb long-range ferroelectric ordering. Although morphological features varied with temperature, no consistent trend was found with Nb content. These findings showed that optimizing both niobium content and synthesis temperature can significantly enhance the ferroelectric properties of PFO thin films.

Author Contributions: Conceptualization, B.B. and V.S.; methodology, A.I.; validation, V.S., A.I. and B.B.; investigation, B.B. and V.S.; writing—original draft preparation, B.B.; writing—review and editing, B.B. and V.S.; All authors have read and agreed to the published version of the manuscript.

Funding: This research received no external funding.

Institutional Review Board Statement: Not applicable.

Informed Consent Statement: Not applicable.

Data Availability Statement: The original contributions presented in the study are included in the article, further inquiries can be directed to the corresponding author.

Conflicts of Interest: The authors declare no conflicts of interest.

References

1. Khan, H.; Ahmad, T. Perspectives and Scope of Abo$_3$ Type Multiferroic Rare-Earth Perovskites. *Chin. J. Phys.* **2024**, *91*, 199–219. [CrossRef]
2. Cao, J.; Yang, B.; Smith, G.; Mahajan, A.; Zhang, H.; Lin, Y.; Yu, C.; Koval, V.; Zhang, D.; Shi, Y.; et al. Establishing Room-Temperature Multiferroic Behaviour in Bismuth-Based Perovskites. *Mater. Des.* **2024**, *248*, 113498. [CrossRef]
3. Palneedi, H.; Annapureddy, V.; Priya, S.; Ryu, J. Status and Perspectives of Multiferroic Magnetoelectric Composite Materials and Applications. *Actuators* **2016**, *5*, 9. [CrossRef]
4. Sharma, S.; Hernández, M.A.; Siqueiros, J.; Herrera, O.R. Recent Advances in Electric Field-Controlled Magnetism Using Perovskite Multiferroic Heterostructures for Spintronics Applications. *Mater. Lett.* **2024**, *371*, 136974. [CrossRef]
5. Wu, J.; Fan, Z.; Xiao, D.; Zhu, J.; Wang, J. Multiferroic Bismuth Ferrite-Based Materials for Multifunctional Applications: Ceramic Bulks, Thin Films and Nanostructures. *Prog. Mater. Sci.* **2016**, *84*, 335–402. [CrossRef]
6. Dedi; Idayanti, N.; Kristiantoro, T.; Alam, G.F.N.; Sudrajat, N. Magnetic Properties of Cobalt Ferrite Synthesized by Mechanical Alloying. *AIP Conf. Proc.* **2018**, *1964*, 20003.
7. Hanif, S.; Hassan, M.; Riaz, S.; Atiq, S.; Hussain, S.S.; Naseem, S.; Murtaza, G. Structural, Magnetic, Dielectric and Bonding Properties of Bimno$_3$ Grown by Co-Precipitation Technique. *Results Phys.* **2017**, *7*, 3190–3195. [CrossRef]
8. López-Alvarez, M.Á.; Silva-Jara, J.M.; Silva-Galindo, J.G.; Reyes-Becerril, M.; Velázquez-Carriles, C.A.; Macías-Rodríguez, M.E.; Macías-Lamas, A.M.; García-Ramírez, M.A.; de Alba, C.A.L.; Reynoso-García, C.A. Determining the Photoelectrical Behavior and Photocatalytic Activity of an H-Ymno$_3$ New Type of Obelisk-Like Perovskite in the Degradation of Malachite Green Dye. *Molecules* **2023**, *28*, 3932. [CrossRef] [PubMed]
9. Watanabe, K.; Nishikawa, M.; Sakaguchi, H.; Veis, M.; Ishibashi, T. Preparation and Characterization of Ymno$_3$ Thin Films by Metal–Organic Decomposition. *Jpn. J. Appl. Phys.* **2023**, *62*, SB1005. [CrossRef]
10. Rahul, M.T.; Chacko, S.K.; Vinodan, K.; Raneesh, B.; Philip, K.A.; Bhadrapriya, B.C.; Bose, B.A.; Kalarikkal, N.; Rouxel, D.; Viswanathan, P.; et al. Multiferroic and Energy Harvesting Characteristics of P(Vdf-Trfe)-Cufe$_2$o$_4$ Flexible Films. *Polymer* **2022**, *252*, 124910. [CrossRef]
11. Shah, J.; Verma, K.C.; Agarwal, A.; Kotnala, R.K. Novel Application of Multiferroic Compound for Green Electricity Generation Fabricated as Hydroelectric Cell. *Mater. Chem. Phys.* **2020**, *239*, 122068. [CrossRef]
12. Singh Pawar, M.; Raj, A.; Singh, A.K.; Tuli, V.; Anshul, A.; Kumar, M. Lead-Free 'Ca' Doped Bi$_{0.80}$la$_{0.20}$feo$_3$ Multiferroic Material for Solar Cell Applications. *Mater. Today Proc.* **2022**, *67*, 713–718. [CrossRef]
13. Kumar, A.; Ortega, N.; Dussan, S.; Kumari, S.; Sanchez, D.; Scott, J.; Katiyar, R. Multiferroic Memory: A Disruptive Technology or Future Technology? *Solid State Phenom.* **2012**, *189*, 1–14. [CrossRef]
14. Ozawa, K.; Nagase, Y.; Katsumata, M.; Shigematsu, K.; Azuma, M. Single or Vortex Ferroelectric and Ferromagnetic Domain Nanodot Array of Magnetoelectric Bife0.9co0.1o3. *ACS Appl. Mater. Interfaces* **2024**, *16*, 20930–20936. [CrossRef] [PubMed]
15. Shen, J.; Cong, J.; Shang, D.; Chai, Y.; Shen, S.; Zhai, K.; Sun, Y. A Multilevel Nonvolatile Magnetoelectric Memory. *Sci. Rep.* **2016**, *6*, 34473. [CrossRef] [PubMed]
16. Kumar, M.; Shankar, S.; Kumar, A.; Anshul, A.; Jayasimhadri, M.; Thakur, O.P. Progress in Multiferroic and Magnetoelectric Materials: Applications, Opportunities and Challenges. *J. Mater. Sci. Mater. Electron.* **2020**, *31*, 19487–19510. [CrossRef]
17. Beklešovas, B.; Stankus, V.; Abakevičienė, B.; Link, J.; Stern, R.; Plyushch, A.; Banys, J.; Čyvienė, J.; Girčys, R.; Bašinskas, M.; et al. Synthesis and Characterization of Cr-Doped Pb$_2$fe$_2$o$_5$ Thin Films by Reactive Magnetron Sputtering. *ECS J. Solid State Sci. Technol.* **2023**, *12*, 103014. [CrossRef]
18. Beklešovas, B.; Stankus, V.; Iljinas, A.; Marcinauskas, L. Ferroelectric and Structural Properties of Cobalt-Doped Lead Ferrite Thin Films Formed by Reactive Magnetron Sputtering. *Crystals* **2024**, *14*, 721. [CrossRef]
19. Beklešovas, B.; Stankus, V.; Iljinas, A.; Balčiūnaitė, U. Enhancement of Ferroelectric Properties of Ni-Substituted Pb$_2$fe$_2$o$_5$ Thin Films Synthesized by Reactive Magnetron Sputtering Deposition. *Coatings* **2025**, *15*, 143. [CrossRef]
20. Choi, E.-S.; Yoon, S.-G.; Choi, W.-Y.; Kim, H.-G. Integration of Platinum Bottom Electrode on Poly-Si for Ferroelectric Thin Films. *Appl. Surf. Sci.* **1999**, *141*, 77–82. [CrossRef]
21. Leclerc, G.; Poullain, G.; Bouregba, R.; Chateigner, D. Influence of the Substrate on Ferroelectric Properties of <111> Oriented Rhombohedral Pb(Zr$_{0.6}$ti$_{0.4}$)O$_3$ Thin Films. *Appl. Surf. Sci.* **2009**, *255*, 4293–4297.
22. Maeder, T.; Sagalowicz, L.; Muralt, P. Stabilized Platinum Electrodes for Ferroelectric Film Deposition Using Ti, Ta and Zr Adhesion Layers. *Jpn. J. Appl. Phys.* **1998**, *37*, 2007. [CrossRef]

23. Millon, C.; Malhaire, C.; Barbier, D. Ti and Tio_x Seeding Influence on the Orientation and Ferroelectric Properties of Sputtered Pzt Thin Films. *Sens. Actuators A Phys.* **2004**, *113*, 376–381. [CrossRef]
24. Gil, D.M.; Nieva, G.; Franco, D.G.; Gómez, M.I.; Carbonio, R.E. Lead Nitroprusside: A New Precursor for the Synthesis of the Multiferroic $Pb_2fe_2o_5$, an Anion-Deficient Perovskite. *Mater. Chem. Phys.* **2013**, *141*, 355–361. [CrossRef]
25. Jun, Y.-K.; Moon, W.-T.; Chang, C.-M.; Kim, H.-S.; Ryu, H.S.; Kim, J.W.; Kim, K.H.; Hong, S.-H. Effects of Nb-Doping on Electric and Magnetic Properties in Multi-Ferroic $Bifeo_3$ Ceramics. *Solid State Commun.* **2005**, *135*, 133–137. [CrossRef]
26. Makhdoom, A.R.; Akhtar, M.J.; Rafiq, M.A.; Siddique, M.; Iqbal, M.; Hasan, M.M. Enhancement in the Multiferroic Properties of $Bifeo_3$ by Charge Compensated Aliovalent Substitution of Ba and Nb. *AIP Adv.* **2014**, *4*, 37113. [CrossRef]
27. Abakumov, A.M.; Hadermann, J.; Bals, S.; Nikolaev, I.V.; Antipov, E.V.; Van Tendeloo, G. Crystallographic Shear Structures as a Route to Anion-Deficient Perovskites. *Angew. Chem. Int. Ed.* **2006**, *45*, 6697–6700. [CrossRef] [PubMed]
28. Wang, M.; Tan, G. Multiferroic Properties of $Pb_2fe_2o_5$ Ceramics. *Mater. Res. Bull.* **2011**, *46*, 438–441. [CrossRef]
29. Arya, K.S.; Kalyani, A.K.; Chakrabarti, T. Flash Sintering of Lead Zirconate Titanate (Pzt) with Minimal Lead Oxide Loss and Enhanced Dielectric Properties. *J. Eur. Ceram. Soc.* **2024**, *44*, 2797–2810. [CrossRef]
30. Hung, C.-L.; Wu, T.-B. Effects of Nb Doping on Highly Fatigue-Resistant Thin Films of $(Pb_{0.8}ba_{0.2})Zro_3$ for Ferroelectric Memory Application. *J. Cryst. Growth* **2005**, *274*, 402–406. [CrossRef]
31. Fisher, J.G.; Jang, S.-H.; Park, M.-S.; Sun, H.; Moon, S.-H.; Lee, J.-S.; Hussain, A. The Effect of Niobium Doping on the Electrical Properties of $0.4(Bi_{0.5}k_{0.5})Tio_{3-0.6}bifeo_3$ Lead-Free Piezoelectric Ceramics. *Materials* **2015**, *8*, 8183–8194. [CrossRef] [PubMed]
32. Xu, D.; Zhao, W.; Cao, W.; Li, W.; Fei, W. Electrical Properties of Li and Nb Modified $Bifeo_3$ Ceramics with Reduced Leakage Current. *Ceram. Int.* **2021**, *47*, 4217–4225. [CrossRef]
33. Cartwright, J.H.E.; Escribano, B.; Piro, O.; Sainz-Diaz, C.I.; Sánchez, P.A.; Sintes, T. Ice Film Morphologies and the Structure Zone Model. *AIP Conf. Proc.* **2008**, *982*, 696–701. [CrossRef]
34. Xian, H.; Tang, L.; Mao, Z.; Zhang, J.; Chen, X. Synergistic Effects of Ca^{2+} and High-Valence Nb^{5+} Co-Doping on the Structural, Optical and Magnetic Properties of $Bifeo_3$. *J. Mater. Sci. Mater. Electron.* **2021**, *32*, 10299–10307. [CrossRef]
35. Barranco, A.; Borras, A.; Gonzalez-Elipe, A.R.; Palmero, A. Perspectives on Oblique Angle Deposition of Thin Films: From Fundamentals to Devices. *Prog. Mater. Sci.* **2016**, *76*, 59–153. [CrossRef]